ELSEVIER

Journal of Molecular Liquids 141 (2008) 110–117

journal of MOLECULAR LIQUIDS

www.elsevier.com/locate/molliq

On the complexity of the absorption spectrum of molecular nitrogen

M.O. Vieitez [a], T.I. Ivanov [a], W. Ubachs [a], B.R. Lewis [b], C.A. de Lange [a,*]

[a] Department of Physics and Astronomy, Laser Centre, Vrije Universiteit, De Boelelaan 1081, 1081 HV Amsterdam, The Netherlands
[b] Research School of Physical Sciences and Engineering, The Australian National University, Canberra, Australian Capital Territory 0200, Australia

Available online 13 February 2008

Abstract

The spectral properties of molecular nitrogen are crucial to a better understanding of radiative-transfer phenomena and activated N/N_2 chemistry in the Earth's upper atmosphere. Excited states of N_2 are difficult to access experimentally, and analysis of its electric dipole-allowed spectrum is notoriously complex. In this paper, we give an overview of these complexities and of the power of extreme ultraviolet ionization spectroscopy in unraveling many of the observed features. Some illustrative examples from our own research will be discussed.

Pacs: 33.20.Ni; 33.20.Sn; 33.80.Gj
Keywords: Molecular nitrogen; Extreme ultraviolet spectroscopy; Predissociation; Perturbations

1. Introduction

The importance of molecular nitrogen as the most abundant species in the Earth's atmosphere is evident. The strong absorption bands in the range 80–100 nm shield the Earth's surface from the extreme ultraviolet (XUV) part of the solar radiation [1]. In fact, even the entire troposphere and stratosphere are free from this hazardous radiation that penetrates only some ~150 km above the Earth's surface. Absorption of the short-wavelength light leads to molecular dissociation, and for N_2 this process is *via* predissociation, with ground- and excited-state atoms as products. Clearly, an understanding of the spectroscopy of N_2 in this wavelength range is essential for a better understanding of radiative-transfer phenomena and activated N/N_2 chemistry in the Earth's upper atmosphere. Similar processes are expected to take place in our solar system in the upper atmospheres of Jupiter, Saturn and its moon Titan, and Triton, the largest moon of Neptune [2].

Molecular nitrogen, N_2, together with the isoelectronic carbon monoxide CO, is one of the most stable molecules in nature. The electronic configuration of homonuclear N_2 in its $X^1\Sigma_g^+$ ground state is:

$$\left(1s\sigma_g\right)^2\left(1s\sigma_u\right)^2\left(2s\sigma_g\right)^2\left(2s\sigma_u\right)^2\left(2p\pi_u\right)^4\left(2p\sigma_g\right)^2,$$

corresponding to a triple chemical bond. For $^{14}N^{15}N$, the g (*gerade*) and u (*ungerade*) symmetry assignments for the orbitals hold only in approximation. The triple chemical bond explains the large dissociation limit of N_2 (78 714 cm^{-1} [3]). Removal of an electron from the highest occupied molecular orbital leads to the lowest $X^2\Sigma_g^+$ ionic state, with configuration

$$\left(1s\sigma_g\right)^2\left(1s\sigma_u\right)^2\left(2s\sigma_g\right)^2\left(2s\sigma_u\right)^2\left(2p\pi_u\right)^4\left(2p\sigma_g\right)^1,$$

and an ionization energy of 125 666.959 cm^{-1} [4]. As a result, excited electronic states of molecular nitrogen are high lying and not easily accessible by normal experimental means.

Focusing on optical transitions involving the ground state, the weak spin-forbidden $A\ ^3\Sigma_u^+–X^1\Sigma_g^+$ Vegard–Kaplan bands, the weak symmetry-forbidden $a'\ ^1\Sigma_u^-–X^1\Sigma_g^+$ Ogawa–Tanaka–Wilkinson–Mulliken and $a\ ^1\Pi_g–X^1\Sigma_g^+$ Lyman–Birge–Hopfield bands have been observed, both in emission and absorption in the (far) ultraviolet (UV) [3]. The weakness of these bands implies that N_2 is optically transparent in the visible and UV regions of the spectrum. The much stronger one-photon electric-dipole-allowed absorption features in the N_2 spectrum involve transitions to valence and Rydberg states of $^1\Sigma_u^+$ and $^1\Pi_u$ symmetry from the ground state and are found in the extreme ultraviolet.

In this paper, we shall focus on the complexities of the electric-dipole-allowed spectrum of molecular nitrogen and on the role that XUV ionization spectroscopy can play in unraveling them. The N_2 spectrum, situated in the energy range just above 100 000 cm^{-1},

* Corresponding author.
E-mail address: cdelange@few.vu.nl (C.A. de Lange).

0167-7322/$ - see front matter © 2008 Elsevier B.V. All rights reserved.
doi:10.1016/j.molliq.2008.01.014

displays many irregularities due to strong global vibronic Rydberg-valence interactions between the singlet ungerade states. Other local and accidental perturbations in the rotational structure are also evident in many places, generally arising from heterogeneous interactions that are usually significantly dependent on the isotopomer involved. All these interactions strongly affect vibronic and rotational intensities, and can result in vibronic and rotational quantum interferences. Another key process is predissociation, which is mediated through the spin-orbit interaction with triplet states. This coupling between the singlet and triplet manifolds is another source of spectral complexity. The rate of predissociation in molecular nitrogen is often sufficiently slow not to wash out the rotational structure in highly-excited states completely, but, at the same time sufficiently fast to allow the observation of line broadening of individual rotational transitions. Because of its excellent spectral resolution, XUV-laser spectroscopy is eminently suitable for resolving this rotational structure and for determining the degree of line broadening and the corresponding rate of predissociation. Various illustrative examples derived from our research in Amsterdam will be discussed.

2. The complexity of the spectrum

The dipole-allowed absorption spectrum of molecular nitrogen in the XUV shows a very complex behavior. Initially, it was thought that the many bands in the spectrum were due to transitions involving a large number of excited electronic states [3], but later it was found that they arose as a result of Rydberg-valence and Rydberg–Rydberg interactions between a limited number of singlet ungerade states lying at excitation energies just above 100 000 cm^{-1} [5,6,7]. There are two valence states involved, one of $^1\Sigma_u^+$ and one of $^1\Pi_u$ symmetry (designated as $b'\,^1\Sigma_u^+$ and $b^1\,\Pi_u$, respectively). The relevant Rydberg states belong either to the series converging on the lowest $X^2\Sigma_g^+$ ionization limit ($np\sigma_u\, c'_{n+1}\,^1\Sigma_u^+$ and $np\pi_u\, c_n\,^1\Pi_u$, with principal quantum number $n \geq 3$), or the $ns\sigma_g\, o_n\,^1\Pi_u$ series, converging on the $A\,^2\Pi_u$ ionic limit of N_2^+. The relevant electronic configurations of the lowest-lying singlet states are:

$b'\,^1\Sigma_u^+ \ldots (2s\sigma_u)^2(2p\pi_u)^3(2p\sigma_g)^2(2p\pi_g)^1$ valence
$b^1\Pi_u \ldots (2s\sigma_u)^1(2p\pi_u)^4(2p\sigma_g)^2(2p\pi_g)^1$ valence
c'_4 or $c'\,^1\Sigma_u^+ \ldots (2s\sigma_u)^2(2p\pi_u)^4(2p\sigma_g)^1(3p\sigma_u)^1$ Rydberg
c_3 or $c^1\Pi_u \ldots (2s\sigma_u)^2(2p\pi_u)^4(2p\sigma_g)^1(3p\pi_u)^1$ Rydberg
o_3 or $o^1\Pi_u \ldots (2s\sigma_u)^2(2p\pi_u)^3(2p\sigma_g)^2(3s\sigma_g)^1$ Rydberg.

Potential-energy curves of these states, together with the C, C', F and G states of triplet character (to be discussed later), are presented in Fig. 1. They have the following configurations:

$C^3\Pi_u \ldots (2s\sigma_u)^1(2p\pi_u)^4(2p\sigma_g)^2(2p\pi_g)^1$ valence
$C'^3\Pi_u \ldots (2s\sigma_u)^2(2p\pi_u)^3(2p\sigma_g)^1(2p\pi_g)^2$ valence
$F^3\Pi_u \ldots (2s\sigma_u)^2(2p\pi_u)^3(2p\sigma_g)^2(3s\sigma_g)^1$ Rydberg
$G^3\Pi_u \ldots (2s\sigma_u)^2(2p\pi_u)^4(2p\sigma_g)^1(3p\pi_u)^1$ Rydberg.

We note, in particular, that the configurations listed above for the b, b', and C valence states are those predominating at smaller internuclear distances R. As R increases, other configurations become important [8], as evidenced by the unusual shapes of the potential-energy curves for these states in Fig. 1.

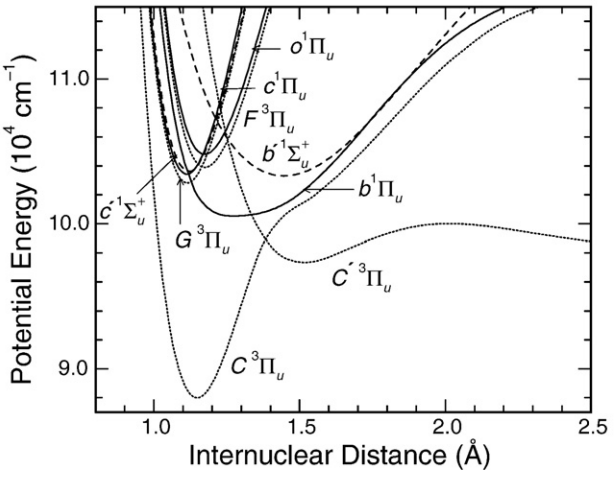

Fig. 1. Potential-energy curves for the ungerade singlet states that govern the dipole absorption spectrum, and the triplet (C, C', F and G) electronic states that govern the predissociation behavior of N_2. Full lines: $^1\Pi_u$ states. Dashed lines: $^1\Sigma_u^+$ states. Dotted lines: $^3\Pi_u$ states.

A detailed understanding of the spectroscopy in this energy region has long been hampered by the complex nature of the observed spectra. In a benchmark paper by Stahel et al. [9], a model of Rydberg-valence interactions was developed that provides a quantitative explanation for the energy-level perturbations, the seemingly erratic behavior of the rotational constants, and the observed band intensities that deviate strongly from Franck–Condon predictions, due to vibronic quantum-interference effects. In particular, the homogeneous vibronic interactions between states of $^1\Sigma_u^+$ symmetry (the b' valence and the c'_4 and c'_5 Rydberg states) and between states of $^1\Pi_u$ symmetry (the b valence and the c_3 and o_3 Rydberg states) were treated [9]. These global perturbations have been crucial in understanding the key features of the allowed optical absorption spectrum of N_2. Later, Spelsberg and Meyer put forward a quantitatively improved model, based on *ab initio* calculations [10]. Edwards et al. [11] extended the model by incorporating heterogeneous interactions to treat the mixing of states with different symmetries. These rotationally-dependent perturbations are local in character, and experimental methods to study such interactions usually require rotational resolution. These perturbations may cause shifts in rotational energy levels and can affect rotational transition intensities and predissociation line widths. Similar to what has been observed in the case of vibronic levels, such interactions may also give rise to rotational quantum interferences.

Photodissociation can occur directly, by photoexcitation from a bound state to a repulsive state or to a bound state above its dissociation limit. Dissociation can also be indirect, when photoexcitation takes place from a bound state to another bound state, which in turn 'predissociates' through a perturbative interaction with the continuum of another electronic state. The importance of predissociation phenomena in the lowest-lying electric-dipole accessible states of the abundant $^{14}N_2$ and its rarer stable isotopomers, $^{14}N^{15}N$ and $^{15}N_2$, has been apparent for

decades [12]. A diversity of experimental techniques was exploited to chart the most prominent of the predissociation effects. Studies of fluorescence excitation, induced either by electron collisions [13] or by synchrotron-radiation absorption [14], revealed the subclass of states that are subject to radiative decay, while the early XUV-laser studies revealed the strongly varying predissociative behavior for vibrational levels within a single electronic manifold [15]. Complementary techniques employing neutralization in fast ion beams allowed for monitoring of the photo-fragments from predissociating N_2 [16,17]. However, a detailed quantitative understanding of the mechanisms underlying N_2 predissociation was not achieved until the work of Lewis et al. [18,19]. This work is based on a coupled-channel Schrödinger equation (CSE) model, and it should be emphasized that it achieves spectroscopic accuracy, therefore allowing for a close comparison with experiment. In essence, the homogeneous ($\Delta\Omega=0$) spin-orbit coupling provides an interaction between accessible singlet states and the triplet manifold. The spin-orbit coupling takes place between $^1\Pi_u$ and $C^3\Pi_u$, which in turn is coupled to $C'^3\Pi_u$ above its dissociation limit. This is a form of accidental (or indirect) predissociation and can be interpreted as a perturbation of a nominally bound rotational level by a predissociated level that lies nearby in energy. The above pathway for predissociation in molecular nitrogen in the region below 105 000 cm^{-1} has been confirmed by a large body of experimental spectroscopic evidence, based on an analysis of global and local perturbations. We note that the present understanding of the predissociation mechanisms for the $^1\Sigma_u^+$ states (with smaller predissociation rates) is not as well developed.

Since predissociation of molecular nitrogen is such a key process, experimental methods suitable for its detection are important. In this paper, we shall show how ionization of N_2 and its isotopomers in a 1 XUV+1′ UV ionization process is a very convenient way of monitoring predissociation with rotational resolution. The method allows for the reliable detection of predissociation rates from experimentally observed line broadening. The excited-state lifetimes in molecular nitrogen happen to be in the range where the rotational structure in the spectra can still be discerned, while the associated line broadening often exceeds the instrumental line widths if narrow-band laser systems are used. Moreover, the interplay between our XUV-laser experiments and the theory, as treated in the CSE model, forms a very powerful and successful combination that has led to significant new insights. As examples, the CSE model was able to explain the strongly varying lifetimes for the $b^1\Pi_u(v=1)$ state in the three N_2 isotopomers [20], and it predicted the location of the very weak spectral lines probing the $F^3\Pi_u(v=0)$ state, that were indeed observed [21].

Since our 1 XUV+1′ UV laser experiments start with molecular nitrogen in its $X^1\Sigma_g^+$ ground state, we are principally limited in what we can learn to detailed studies of the singlet ungerade manifold. Our studies are concerned with rotationally resolved interactions between states that lead to perturbed term energies and transition intensities. These perturbations can take the form of rotational quantum interferences, similar to the vibronic quantum interferences discussed in [9]. However, important information about the triplet manifold can also be collected, both directly and indirectly, since spin-orbit coupling with triplets can cause observable perturbations in the singlet manifold. When the focus is on rotationally resolved phenomena, these perturbations are usually isotopomer-dependent. Hence, the experimental study of the different stable isotopomers tends to be very informative.

As illustrative examples from our own research, we shall discuss the analysis of homogeneous and heterogeneous perturbations in the singlet manifold, rotationally resolved quantum interferences in oscillator strengths and predissociation line widths, and the direct and indirect observation of triplet states through their interactions with the singlet manifold.

3. Experimental

Details of the experimental method, including a description of the lasers, vacuum setup, molecular-beam configuration, time-of-flight (TOF) detection scheme and calibration procedures, have been given previously [22]. A skimmed and well defined pulsed molecular beam of nitrogen is perpendicularly intersected by temporally and spatially overlapping the XUV and UV laser beams. Nitrogen molecules are resonantly excited by the XUV photons and subsequently ionized by the intense UV light. N_2^+ ions are detected using a TOF mass selector.

For the detailed investigation of the N_2 spectral features, a tunable light source in the extreme ultraviolet region with sufficiently narrow bandwidth is required. Tunability and narrow bandwidth are achieved using two types of laser sources which deliver energetic pulses in the visible wavelength domain. Harmonic generation in two steps, by frequency doubling in nonlinear crystals and subsequent frequency tripling in gas jets, provides coverage of the XUV wavelength range, while the bandwidth of the fundamental light sources is nearly retained in the conversion process. When using a commercially available Pulsed Dye Laser (PDL), the bandwidth in the XUV is ~0.3 cm^{-1} full-width at half-maximum (FWHM) and the absolute wavenumber uncertainty in the XUV for this system is ±0.1 cm^{-1} for fully-resolved lines. When using a home-built Pulsed Dye Amplification system, a bandwidth of ~0.01 cm^{-1} FWHM is attained and the absolute calibration uncertainty is ±0.005 cm^{-1}. Wavelength calibration can be performed in the visible range, since exact harmonics are produced in the nonlinear optical conversion process.

The two-photon-ionization TOF experiment has some useful characteristics that are favorably employed. Mass separation can be combined with laser excitation to separate the contributions to the spectrum of the main $^{14}N_2$ isotopomer from those of the $^{14}N^{15}N$ and $^{15}N_2$ species. Furthermore, by changing the relative delay between the N_2 pulsed-valve trigger and the laser pulse, as well as varying the nozzle-skimmer distance, the rotational temperature in the molecular beam can be selected to measure independent spectra of cold (10–20 K) and warm (up to 300 K) samples. This form of temperature tuning of the gaseous sample aids in the assignment of the spectral lines.

In a 1 XUV+1′ UV two-photon-ionization experiment, the excited state is populated by the XUV absorption process and depopulated by decay mechanisms that all, in principle, lead to

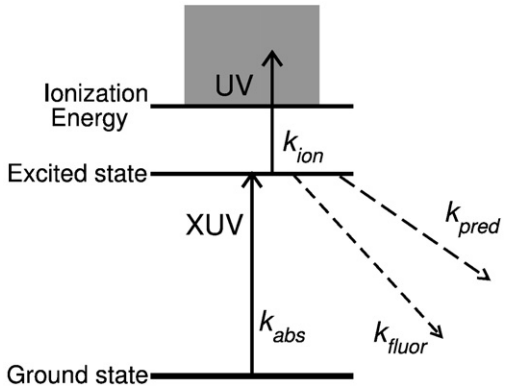

Fig. 2. Competing decay mechanisms in a 1 XUV + 1′ UV ionization experiment. The XUV photon excites the molecule with rate k_{abs}. From the excited state, the molecule can fluoresce to lower levels with rate k_{fluor}, it can undergo predissociation (with rate k_{pred}) or, *via* a UV photon, it can become ionized. This ionization process is, in principle, non resonant and it occurs with rate k_{ion}.

a shortened lifetime (see Fig. 2). This occurs through (i) fluorescence, (ii) predissociation, and (iii) through ionization by UV radiation. As we intend to measure line widths with our setup, excessive UV radiation that would lead to depletion of the population of the intermediate state is avoided in our experiment. Information on predissociation can be obtained using several complementary methods. The lifetime τ (s) of the excited level, shortened due to predissociation, can be expressed as $\tau = (2\pi c\Gamma)^{-1}$, with Γ the natural (Lorentzian) line width (in cm^{-1} FWHM). Hence, the excited-state lifetime τ can be derived straightforwardly from line-width measurements. The shortening of the lifetime due to predissociation will not only cause line broadening, but also a decrease in signal intensity, since we detect ions that result from ionization of a decaying excited level. Using a rate equation model [23], it can be proved that the intensity of the signal is proportional to the lifetime of the excited state, when the laser line width exceeds the natural width Γ.

Hence, predissociation can be monitored by (i) directly detecting the broadening of the XUV transition [15]; (ii) carrying out a pump-probe experiment on the excited state with a variable time delay between the pulses [24]; (iii) measuring the decrease in the ionization signal which is proportional to the decrease of the excited-state lifetime; or (iv) measuring the decrease in the fluorescence signal. In our experiments, both the decrease in the ionization signal and the broadening of the excited-state line width are signatures of the occurrence of predissociation.

4. Illustrative examples

In this section we shall treat a number of examples of (i) homogeneous interactions between states of the same symmetry and heterogeneous interactions between states of different symmetry; (ii) quantum-interference effects occurring both in the oscillator strengths between electric-dipole allowed transitions, and in the line widths between predissociating levels; and (iii) evidence for triplet states through their coupling with the singlet manifold. Without trying to be exhaustive, we have selected these examples from our research as representative of the current experimental and theoretical state-of-the-art in studying perturbation and predissociation phenomena in molecular nitrogen.

4.1. The $o^1\Sigma_u^+(v=1)\sim b^1\Pi_u(v=9)\sim b'^1\Sigma_u^+(v=6)$ interaction complex in $^{14}N_2$

In the energy region between 107 000 and 108 000 cm^{-1}, the following energy levels in $^{14}N_2$ are situated closely together, thus allowing for possible interactions: $o^1\Sigma_u^+(v=1)$ (Rydberg), and the valence states $b^1\Pi_u(v=9)$ and $b'^1\Sigma_u^+(v=6)$. For $^{14}N_2$ at low J values, the $o(v=1)$ and $b(v=9)$ states cross, while at higher J values this complex can interact with the $b'(v=6)$ state. In Fig. 3, the $b^1\Pi_u$–$X^1\Sigma_g^+(9,0)$ and $o^1\Pi_u$–$X^1\Sigma_g^+(1,0)$ high-temperature spectra are presented, showing the P, Q, and R branches. For the isotopomers $^{14}N^{15}N$ and $^{15}N_2$, the relative positions of the $o(v=1)$ and $b(v=9)$ states are such that significant interactions are not expected between these states.

Rotational levels associated with excited states can be of e or f parity in the case of $^1\Pi_u$ states, or only of e parity for $^1\Sigma_u^+$. Moreover, in $^1\Pi_u$ states, Λ-doubling occurs. These issues are discussed in detail in many places [25,26]. In order to obtain the term energies and transition intensities, a detailed analysis must be carried out. First, the rotational transitions P, Q and R are assigned, guided by the nuclear spin statistics, the combination differences (for the P and R branches) and the differences in intensities from the cold and warm spectra. These experimental transition energies are then compared with theoretical values calculated using ground- and upper-state term values which are parameterized employing the usual spectroscopic parameters (rotational constant B, centrifugal distortion parameters D and H). The rotational level structure of the ground state is well understood and represented by the constants published by Trickl et al. [27] in the case of $^{14}N_2$, and by the constants of Bendtsen

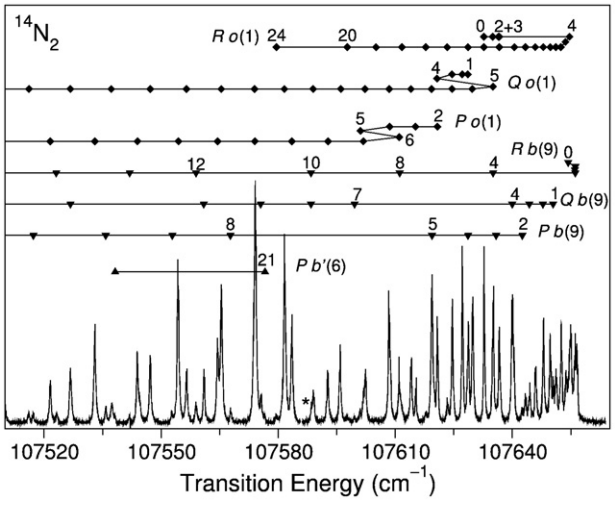

Fig. 3. PDL-based XUV-source spectra of the $b^1\Pi_u$–$X^1\Sigma_g^+(9,0)$ and $o^1\Pi_u$–$X^1\Sigma_g^+(1,0)$ bands of $^{14}N_2$, with corresponding line assignments. Two separate scans are joined in the region marked with an asterisk (*), and their relative intensities should not be compared. Note that several lines are blended and many transitions are too weak to be observed.

et al. [28] for the other isotopomers. By adjusting the upper-state rotational constants to minimize the differences with respect to the experimental transitions, a least-squares fit of the rotational constants and therefore of the term values is obtained.

The $b^1\Pi_u$ (v=9) and $o^1\Pi_u$ (v=1) levels in $^{14}N_2$ undergo an avoided crossing in the rotational structure between J=4 and J=5. Since both states have the same symmetry, this interaction is homogeneous ($\Delta\Omega$=0), electrostatic in character, J-independent and involves both the e- and f-parity levels. Moreover, at high J an interaction that only involves e-parity levels between $b'^1\Sigma_u^+$ (v=6) and $o^1\Pi_u$ (v=1) is apparent. This interaction is heterogeneous ($\Delta\Omega\neq0$), arises from **L**-uncoupling and is therefore J-dependent. For the e-parity levels, a complete three-state deperturbation was performed for each value of J by diagonalizing the matrix

$$\begin{pmatrix} T_{b9}(J) & H_{b9o1} & 0 \\ H_{b9o1} & T_{o1}(J) & H_{o1b'6}\sqrt{J(J+1)} \\ 0 & H_{o1b'6}\sqrt{J(J+1)} & T_{b'6}(J) \end{pmatrix}. \quad (1)$$

The diagonal elements are the term energies of the b(v=9), o (v=1) and b'(v=6) states. The off-diagonal element H_{b9o1} is the homogeneous interaction between the $^1\Pi_u$ states, and $H_{o1b'6}\sqrt{J(J+1)}$ represents the effective heterogeneous interaction matrix element between o(v=1) and b'(v=6). For f-parity levels, Eq. (1) reduces to a 2×2 matrix.

In Fig. 4, the e-parity term values, reduced such that the deperturbed b(v=9) values lie on the zero line, are shown. The figure clearly shows an avoided crossing between J=4 and J=5 for the b(v=9) and o(v=1) states, with a maximum energy shift of 8.7 cm^{-1} at J=4. A second avoided crossing, this time between o(v=1) and b'(v=6), occurs between J=24 and J=25, with a maximum shift of 13.5 cm^{-1} at J=25. A similar f-parity plot can be constructed for the coupling between the Rydberg and valence $^1\Pi_u$ states.

Moreover, around the rotational levels where the interaction takes place, the wave functions are strongly mixed. For each

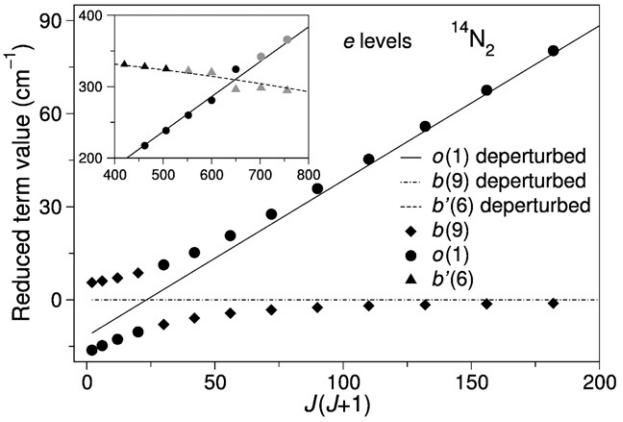

Fig. 4. Term values of the $b^1\Pi_u(v=9)\sim o^1\Pi_u(v=1)\sim b'^1\Sigma_u^+(v=6)$ e-parity states, reduced such that the deperturbed b(v=9) levels are on the zero line. Clear anti-crossings for the $b(v=9)\sim o(v=1)$ and $o(v=1)\sim b'(v=6)$ levels are shown. Measured energy levels are displayed using black symbols, predicted levels using grey symbols.

state, the wave function will be a linear combination of the unperturbed wave functions:

$$\Psi = c_1\Phi_{o(1)} + c_2\Phi_{b(9)} + c_3\Phi_{b'(6)}, \quad (2)$$

where the values of the c_i coefficients are the components of the eigenvectors of Eq. (1). Near J=4, o(v=1) and b(v=9) exchange electronic character, while the level of mixing of b' (v=6) is almost negligible. The wave functions of o(v=1) and b (v=9) are then expressed as:

$$\Psi_{o(1)} = c\Phi_{o(1)} + \sqrt{1-c^2}\Phi_{b(9)},$$

$$\Psi_{b(9)} = -\sqrt{1-c^2}\Phi_{o(1)} + c\Phi_{b(9)}. \quad (3)$$

Also, near J=25, the same happens for the e-levels of o(v=1) and b'(v=6), while the mixing of b(v=9) is close to zero. For the intermediate J levels, a three-state problem can be solved.

4.2. Rotational quantum-interference effects

4.2.1. Oscillator strengths

Because both the $b-X$(9,0) and $o-X$(1,0) transitions carry oscillator strength, and since both b(v=9) and o(v=1) levels of like symmetry interact, this leads to a classic situation where two-level quantum-interference effects are expected. As discussed by Lefebvre–Brion and Field [25], the perturbed vibronic oscillator strengths for transitions from a common level 0 (the $X^1\Sigma_g^+$ ground state in our case) to upper (+) and lower (−) levels of the interacting pair are given by:

$$f_{+0} = c^2 f_{10} + \left(1-c^2\right) f_{20} \pm 2c\sqrt{(1-c^2) f_{10} f_{20}},$$

$$f_{-0} = \left(1-c^2\right) f_{10} + c^2 f_{20} \mp 2c\sqrt{(1-c^2) f_{10} f_{20}}, \quad (4)$$

where f_{10} and f_{20} are the vibronic oscillator strengths for transitions to the unperturbed levels 1 and 2, and $c>0$ signifies the mixing coefficient that corresponds to the amount of character of the unperturbed level 1 in the perturbed upper-level wave function, as explained previously. Using the mixing coefficients that have been obtained from the deperturbation procedure in the previous section, we can now deperturb the experimental oscillator strengths through the application of Eq. (4).

Our 1 XUV+1′ UV experiments reveal perturbations in the intensity pattern of the observed transitions, but as the photon flux is not measured, and the ionization cross sections are not known *a priori*, absolute oscillator strengths are not obtainable with our setup. Therefore, recent synchrotron-based measurements are used [26] (see also [29]) and shown in Fig. 5. As is apparent from the figure, transitions to the higher-energy level, i.e., b(v=9) for $J\leq4$ and o(v=1) for $J\geq5$, show a strong rotational dependence and peak around J=6. At the same time, oscillator strengths to the lower-energy level, i.e., o(v=1) for $J\leq4$ and b(v=9) for $J\geq5$, show a minimum at J=6, to the extent that this transition was too weak to be observed. Deperturbation of the experimental oscillator strengths according to Eq. (4) leads to the dot-dashed line in Fig. 5 for the $o-X$(1,0) transition, and to the long-dashed

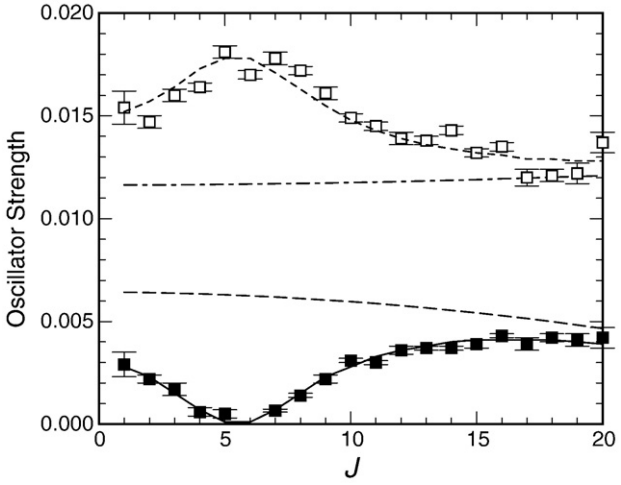

Fig. 5. Rotational dependence of band oscillator strengths (obtained from synchrotron-based experiments [26]) in the mixed $b-X(9,0)$ and $o-X(1,0)$ transitions of $^{14}N_2$, demonstrating a strong quantum-interference effect near $J=6$, together with the results of a deperturbation analysis (see text). Open squares: experimental (perturbed) oscillator strengths for transitions to the higher-energy levels. Solid squares: experimental oscillator strengths for transitions to the lower-energy levels. Dot-dashed line: deperturbed oscillator strength for the $o-X(1,0)$ transition. Long-dashed line: deperturbed oscillator strength for the $b-X(9,0)$ transition. Dashed curve: calculated perturbed oscillator strength for the higher levels. Solid curve: calculated perturbed oscillator strength for the lower levels.

line for the $b-X(9,0)$ transition. In summary, the experimental oscillator strengths of both bands show clear evidence of rotationally-dependent constructive and destructive quantum-interference effects in $^{14}N_2$. A full account of this work is presented in Ref. [26].

4.2.2. Predissociation line widths

If two energy levels predissociate *via* the same perturbative state, an interaction between these levels may result in a quantum-interference effect in the strength of the predissociation, in the same fashion as for the oscillator strengths. The predissociation strength can be detected *via* line broadening of the measured transitions. In this case, the width interference is described by equations similar to Eq. (4), but with the oscillator strength f replaced by the width Γ, and with 0 the perturbative state. The constructive and destructive interferences observed near $J=6$ for the oscillator strengths of the $b-X(9,0)$ and $o-X(1,0)$ transitions support the notion of line-width interferences and associated predissociation rate modulations. This is actually observed for the $o(v=1)$ and $b(v=9)$ levels. A complete description of this phenomenon is presented in Ref. [26].

4.3. Triplet-singlet interactions

As mentioned above, in principle our setup only allows the direct measurement of singlet ungerade states of N_2. Nevertheless, direct measurement of transitions of the triplet manifold is possible if these transitions become visible *via* intensity borrowing [25]. This is the case for the $F^3\Pi_u(v=0)$ Rydberg state. Sprengers et al. presented the results of an ultrahigh-resolution laser-spectroscopic study of the $F-X(0,0)$ transition

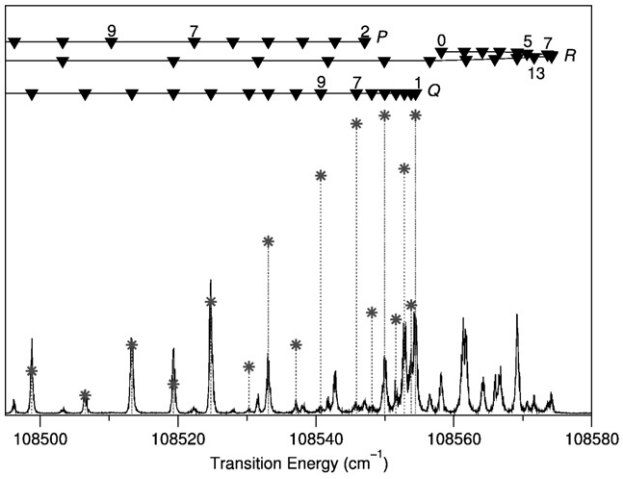

Fig. 6. 1 XUV+1′ UV ionization spectrum for the $c_3{}^1\Pi_u$–$X^1\Sigma_g^+(2,0)$ band of $^{15}N_2$, with corresponding line assignments. The asterisks (∗) indicate how large transition intensities would have been (on a relative scale) if not affected by the singlet-triplet interaction.

in $^{14}N_2$ [21]. This dipole-forbidden transition became observable through the spin-orbit-induced intensity borrowing from the dipole-allowed $b-X(5,0)$ transition. This phenomenon was facilitated by the near-degeneracy of the $F(v=0)$ and $b(v=5)$ levels in the $^{14}N_2$ isotopomer. Direct observation of the F state led to assignments of the R, P and Q branches for the $\Omega=0,1,2$ triplet sublevels, together with the predissociation widths of the transitions. The obtained rotational parameters, together with the term values of the predissociating levels, suggest strong interactions among the F and $G^3\Pi_u$ Rydberg and $C'^3\Pi_u$ valence states. Hence, the complexity of the triplet manifold is somewhat similar to that of the singlet states.

Even when the fortuitous coincidence of energy levels does not allow their direct observation through intensity borrowing effects, the triplet states may manifest themselves in an indirect way, *via* perturbations of the singlet states. In the energy range 108 500–109 500 cm^{-1}, several singlet states, i.e., the Rydberg states $c_3{}^1\Pi_u(v=2)$ and $c_4'{}^1\Sigma_u^+(v=2)$ and the valence states $b'^1\Sigma_u^+(v=7)$ and $b^1\Pi_u(v=11)$ are situated. The predictions of the

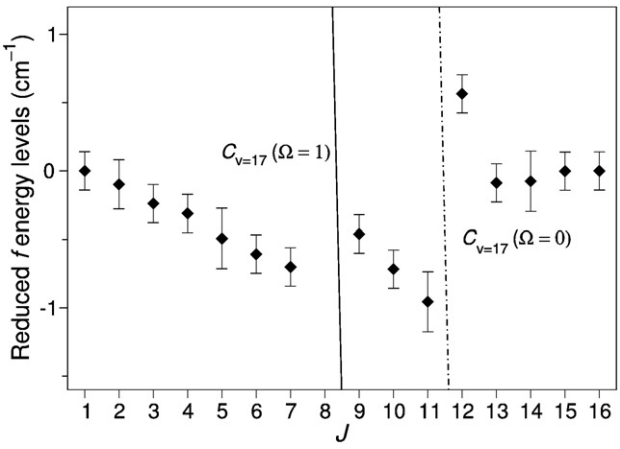

Fig. 7. Energies of the $c_3{}^1\Pi_u(v=2)$ f-parity state of $^{15}N_2$, reduced to be positioned on the zero-energy line. The straight lines indicate the crossings with $C^3\Pi_u(v=17)$ as predicted by an extended model based on [18].

CSE model indicate a crossing between the singlet $c_3\,{}^1\Pi_u(v=2)$ state and the three components ($\Omega=2,1,0$) of the triplet $C^3\Pi_u$ ($v=17$) valence state.

For $^{15}N_2$, the crossing is predicted to occur at relatively low J. This is favorable, because it means that, with the 1 XUV+1′ UV setup, where the lower-J lines show the most intensity, this phenomenon can be detected. For $^{14}N^{15}N$ and $^{14}N_2$, the crossing takes place at higher values of J, that are difficult to access with our XUV setup. In the following, we shall focus on $^{15}N_2$.

The $c_3\,{}^1\Pi_u$–$X^1\Sigma_g^+$ (2,0) band between $J=5$ and $J=13$ shows large intensity deviations from those expected for a Boltzmann distribution. These deviations are apparent in the P, Q, and R branches, shown in Fig. 6. It was found that the $c_3(v=2)$ state interacts with the $b'(v=7)$ state *via* heterogeneous coupling and that the states exchange electronic character around $J=20$. At higher J values, this complex possibly interacts with the $b(v=11)$ state, but the results at higher J for all states did not allow for definitive conclusions. As mentioned before, the heterogeneous interaction involves only e-parity levels, and therefore does not show up in Q-branch transitions. Hence, this intensity depletion is attributed to the crossing with the triplet state.

After the perturbations in the singlet manifold have been accounted for, remaining spectral deviations can be ascribed to the interaction with $C^3\Pi_u(v=17)$. In Fig. 7, the reduced f-parity levels of $c_3(v=2)$ are shown. Similar results were obtained for the e-parity levels. Between $J=7$ and $J=9$, and also between $J=11$ and $J=12$, two perturbations are clearly present. These J-value positions coincide approximately with the predicted crossings with $C^3\Pi_u(v=17)$. In principle, only $C_{\Omega=1}(v=17)$ can interact *via* the homogeneous ($\Delta\Omega=0$) spin-orbit coupling with $c_3(v=2)$. However, since the **S**-uncoupling mechanism induces mixing between the three $C_\Omega(v=17)$ components, all three states can interact to some extent with $c_3(v=2)$. The perturbation between $J=7$ and $J=8$ is assigned to $C_{\Omega=1}$ ($v=17$), and the one between $J=11$ and $J=12$ to $C_{\Omega=0}(v=17)$. No clear indications for a crossing with $C_{\Omega=2}(v=17)$ are observed, but they are expected to occur at lower J values.

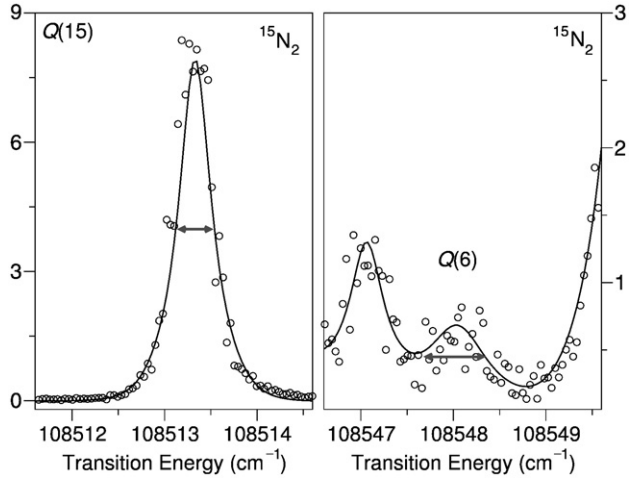

Fig. 8. 1 XUV+1′ UV ionization spectra of the $Q(15)$ and $Q(6)$ lines of the $c_3\,{}^1\Pi_u$–$X^1\Sigma_g^+(2,0)$ band for $^{15}N_2$, recorded using the PDL-based XUV source and showing that $Q(6)$ is a factor of two broader than $Q(15)$, due to the increase of predissociation. Note that the relative X-scales are the same in each subfigure.

In Fig. 8, the line widths for two transitions from the ground state to levels with f parity of the $c_3\,{}^1\Pi_u(v=2)$ state in $^{15}N_2$ are shown. Near $J=8$ and $J=12$, an increase in broadening, and hence in predissociation rates, is observed that is again ascribed to a coupling with the crossing, strongly predissociated $C_\Omega(v=17)$ states. As an example, the line width of $Q(6)$ is increased by predissociation and is approximately double that of $Q(15)$ which shows no broadening beyond the normal Doppler width. Notably, the intensity depletions shown in Fig. 6 take place at the same J values at which the crossings with the triplet states are predicted. Altogether, these results are taken as convincing cumulative evidence that the local interactions with the $C^3\Pi_u(v=17)$ triplet state can be observed indirectly, through their perturbative effects on the singlet manifold. Moreover, the predictions of the CSE model appear to be very adequate in this respect.

5. Conclusions and outlook

In this paper, some of the complexities observed in the electric-dipole-allowed spectrum of molecular nitrogen are discussed. These complexities arise from global vibronic and local rotationally-dependent perturbations, causing energy level shifts, redistribution of intensities and intensity borrowing, and quantum-interference phenomena. Experimental methods, such as XUV ionization spectroscopy, that can achieve rotational resolution are a suitable tool to study this important molecule. The rate of predissociation in molecular nitrogen is often fast enough to cause line broadening that exceeds the narrow-band XUV-laser instrumental line width, but predissociation rates are often slow enough not to remove the rotational structure completely. The triplet manifold plays a key role in the predissociation processes in molecular nitrogen. The continuous interplay with the theoretical CSE modeling that is essentially capable of spectroscopic accuracy has played a crucial role in the detailed analysis and understanding of our experimental results.

The connection between high-resolution XUV spectroscopy of the lowest ungerade states of molecular nitrogen and atmospheric chemistry is a strong one. For example, the effective emission from $c_4'^1\Sigma_u^+$–$X^1\Sigma_g^+(0,0)$ and (0,1) bands in the Earth's airglow are unusually weak. The radiation of the (0,0) band, which is in fact the strongest emission feature in the N_2 spectrum [13], is radiatively trapped and undergoes resonant fluorescent scattering under atmospheric conditions. In this process the (0,1) band acquires some intensity also. This (0,1) band is in accidental resonance with the transition $b^1\Pi_u$–$X^1\Sigma_g^+(2,0)$. Since the $b(v=2)$ level is strongly predissociated, the observed overall emission is unexpectedly weak [30]. This remarkable coincidence in the complex N_2 spectrum is strongly dependent on isotopomer, as are many other observed predissociation phenomena in molecular nitrogen [20]. So far, isotopic fractionation in nitrogen-containing atmospheres has been studied principally from the perspective of gravitational phenomena. Dissociative recombination of N_2^+ and electron-impact dissociation of neutral N_2 produce kinetically-hot atomic nitrogen, that, depending on the planetary escape velocities, may lead to isotopic fractionation and strongly varying $^{15}N/^{14}N$ ratios [2,31]. The isotope-dependent predissociation effects resulting from the complexities in the N_2 spectrum will add

to this behavior, although the particularities of each case are to be explored in more detail.

Although fundamental in character, studies of perturbation and predissociation processes in molecular nitrogen and their isotopomers are crucial to a better understanding of radiative-transfer phenomena and activated N/N_2 chemistry in the Earth's upper atmosphere. In a similar spirit, this type of research has implications for other planetary systems with nitrogen-containing atmospheres. For example, Liang et al. [32] have already used the results of a CSE model of N_2 photodissociation to explain nitrogen isotope anomalies in HCN in the atmosphere of Titan.

Future work will attempt to expand both the experimental database and the accurate theoretical modeling to higher energies. This requires the incorporation into the model of a plethora of higher-lying Rydberg and valence states of singlet as well as triplet character, and the interactions among them.

Acknowledgment

Part of this research was supported by Australian Research Council Discovery Program Grant DP0558962.

References

[1] R.R. Meier, Space Sci. Rev. 58 (1991) 1.
[2] T.C. Owen, Planet. Space Sci. 48 (2000) 747.
[3] A. Lofthus, P.H. Krupenie, J. Phys. Chem. Ref. Data 6 (1977) 113.
[4] T. Trickl, E.F. Cromwell, Y.T. Lee, A.H. Kung, J. Chem. Phys. 91 (1989) 6006.
[5] H. Lefebvre-Brion, Can. J. Phys. 47 (1969) 541.
[6] K. Dressler, Can. J. Phys. 47 (1969) 547.
[7] P.K. Carroll, C.P. Collins, Can. J. Phys. 47 (1969) 563.
[8] H.H. Michels, Adv. Chem. Phys. 45 (1981) 225.
[9] D. Stahel, M. Leoni, K. Dressler, J. Chem. Phys. 79 (1983) 2541.
[10] D. Spelsberg, W. Meyer, J. Chem. Phys. 115 (2001) 6438.
[11] S.A. Edwards, W.-Ü.L. Tchang-Brillet, J.-Y. Roncin, F. Launay, F. Rostas, Planet. Space Sci. 43 (1995) 67.
[12] M. Leoni, K. Dressler, J. Appl. Math. Phys. (ZAMP) 22 (1971) 794.
[13] J.M. Ajello, G.K. James, B.O. Franklin, D.E. Shemansky, Phys. Rev. A 40 (1989) 3524.
[14] H. Oertel, M. Kratzat, J. Imschweiler, T. Noll, Chem. Phys. Lett. 82 (1981) 552.
[15] W. Ubachs, L. Tashiro, R.N. Zare, Chem. Phys. 130 (1989) 1.
[16] C.W. Walter, P.C. Cosby, H. Helm, Phys. Rev. A 50 (1994) 2930.
[17] A.B. van der Kamp, P.C. Cosby, W.J. van der Zande, Chem. Phys. 184 (1994) 319.
[18] B.R. Lewis, S.T. Gibson, W. Zhang, H. Lefebvre-Brion, J.M. Robbe, J. Chem. Phys. 122 (2005) 144302.
[19] B.R. Lewis, S.T. Gibson, J.P. Sprengers, W. Ubachs, A. Johansson, C.-G. Wahlström, J. Chem. Phys. 123 (2005) 236101.
[20] J.P. Sprengers, W. Ubachs, K.G.H. Baldwin, J. Chem. Phys. 122 (2005) 144301.
[21] J.P. Sprengers, E. Reinhold, W. Ubachs, K.G.H. Baldwin, B.R. Lewis, J. Chem. Phys. 123 (2005) 144315.
[22] J.P. Sprengers, W. Ubachs, K.G.H. Baldwin, B.R. Lewis, W.-Ü.L. Tchang-Brillet, J. Chem. Phys. 119 (2003) 3160.
[23] K.S.E. Eikema, W. Hogervorst, W. Ubachs, Chem. Phys. 181 (1994) 217.
[24] J.P. Sprengers, A. Johansson, A. L'Huillier, C.-G. Wahlström, B.R. Lewis, W. Ubachs, Chem. Phys. Lett. 389 (2004) 348.
[25] H. Lefebvre-Brion, R.W. Field, The Spectra and Dynamics of Diatomic Molecules, Elsevier, Amsterdam, 2004.
[26] M.O. Vieitez, T.I. Ivanov, J.P. Sprengers, C.A. de Lange, W. Ubachs, B.R. Lewis, G. Stark, Mol. Phys. 105 (2007) 1543.
[27] T. Trickl, D. Proch, K.L. Kompa, J. Mol. Spectrosc. 171 (1995) 374.
[28] J. Bendtsen, J. Raman Spectrosc. 32 (2001) 989.
[29] G. Stark, K.P. Huber, K. Yoshino, P.L. Smith, K. Ito, J. Chem. Phys. 123 (2005) 214303.
[30] M.H. Stevens, R.R. Meier, R.R. Conway, D.F. Strobel, J. Geophys. Res. 99 (1994) 417.
[31] H. Lammer, W. Stumptner, G.J. Molina-Cuberos, S.J. Bauer, T. Owen, Planet. Space Sci. 48 (2000) 529.
[32] M.C. Liang, A.N. Heays, B.R. Lewis, S.T. Gibson, Y.L. Yung, Astrophys. J. 664 (2007) L115.